Estimation of the thermal resistance of a building wall with inverse techniques based on rapid active in situ measurements and white-box or ARX black-box models

Adrien François, Laurent Ibos, Vincent Feuillet, Johann Meulemans

▶ **To cite this version:**

Adrien François, Laurent Ibos, Vincent Feuillet, Johann Meulemans. Estimation of the thermal resistance of a building wall with inverse techniques based on rapid active in situ measurements and white-box or ARX black-box models. Energy and Buildings, 2020, 226, pp.110346. 10.1016/j.enbuild.2020.110346 . hal-03146505

HAL Id: hal-03146505
https://hal.science/hal-03146505

Submitted on 19 Feb 2021

HAL is a multi-disciplinary open access archive for the deposit and dissemination of scientific research documents, whether they are published or not. The documents may come from teaching and research institutions in France or abroad, or from public or private research centers.

L'archive ouverte pluridisciplinaire **HAL**, est destinée au dépôt et à la diffusion de documents scientifiques de niveau recherche, publiés ou non, émanant des établissements d'enseignement et de recherche français ou étrangers, des laboratoires publics ou privés.

Energy & Buildings 226 (2020) 110346, https://doi.org/10.1016/j.enbuild.2020.110346

Estimation of the thermal resistance of a building wall with inverse techniques based on rapid active *in situ* measurements and white-box or ARX black-box models

Adrien François*[1,2], Laurent Ibos[1], Vincent Feuillet[1], and Johann Meulemans[2]

[1]Université Paris-Est Créteil, CERTES, F-94010 Créteil, France
[2]Saint-Gobain Research Paris, 39 quai Lucien Lefranc, F-93303 Aubervilliers, France

July 30, 2020

Abstract

Classical *in situ* measurement methods of building wall thermal resistance are based on steady-state assumptions. This limits their applicability given their high sensitivity to outdoor conditions and the duration required to obtain accurate results. To overcome these limitations, the present paper introduces an *in situ* method for the assessment of building wall thermal resistance. It is based on rapid active measurements: indoor air is heated for several hours. In addition, unlike common active methods based only on temperatures, the proposed method is based on measurements of a heat flux and one or several temperatures. Two approaches are implemented and compared to estimate wall thermal characteristics from measurements. In the first approach, inverse technique are used based on "white-box" models derived from the heat equation. The best direct model to choose depends on the type of wall tested and weather conditions. In the second approach, ARX "black-box" models are used. The proposed methods were thoroughly tested on a full-size load-bearing wall equipped with a classical internal insulation system commonly found in french buildings. The wall was built inside a climate chamber in order to assess the robustness of the methods to various outdoor conditions. The results demonstrated that, for type of wall, both approaches lead to accurate and repeatable results if the external temperature remains roughly constant. With varying external conditions, white-box models remained accurate while ARX "black-box" models did not.

Keywords— *in situ*; measurements; building wall; thermal resistance; inverse methods; ARX

*corresponding author: adrien.francois@u-pec.fr

Nomenclature

Acronyms

ARMA	Auto-Regressive with Moving Average
ARX	Auto-Regressive with eXogenous input
HFM	Heat Flux Meter
HLC	Heat Loss Coefficient
IRT	Infrared Thermography
MISO	Multiple Inputs, Single Output
OLS	Ordinary Least Squares
SISO	Single Input, Single Output

Greek Symbols

α	polynomial coefficient	
$\boldsymbol{\beta}$	parameter vector (white-box)	
$\boldsymbol{\theta}$	parameter vector (ARX)	
Γ	gamma function	
λ	Lagrange weighting factor	
ω	pulsation	$rad.s^{-1}$
ε	noise	
φ	heat flux	$W.m^{-2}$

Roman Symbols

b	thermal effusivity	$J.K^{-1}.m^{-2}.s^{-1/2}$
h	total heat transfer coefficient	$W.m^{-2}.K^{-1}$
k	layer index	
M	thermal quadrupole matrix	
N	number of points	
n	polynomial order	
p	Laplace variable	s^{-1}
R	thermal resistance	$m^2.K.W^{-1}$
T	temperature	K
t	time	s
u	uncertainty	
X^*	reduced sensitivity coefficient	

Superscripts

$\sim$	Laplace transform
$\wedge$	estimated value

Subscripts

e	external
i	internal
in	internal interface
mo	model
s	surface

1 Introduction

The European Union (EU) 2030 climate & energy framework set three main targets to fight against global warming: 40% cuts in greenhouse gas emissions (from 1990 levels), 31% share for renewable energy, and 32.5% improvement in energy efficiency. In addition, residential and non-residential buildings account for about 40% of total energy consumption in the EU [1]. The building sector has therefore a major role to play to reach these goals and minimize our environmental footprint.

Many research projects focus on the minimization of building energy consumption. It was shown that one of the most effective solutions, both for construction and renovation, are to increase the thermal insulation of the envelope. In this context, it is important to assess the thermal performance of buildings. The estimation of these performances is usually based on theoretical calculations and sometimes on numerical simulations. When *in situ* measurements are undertaken, the results often show some discrepancies with predictions. This is the so-called "performance gap" (see [2], [3] and references therein). The mismatch between theory and practice may have various origins such as material properties difference, aging, thermal bridging, moisture and quality of construction. In order to correctly address issues related to the "performance gap", knowledge of the overall building energy losses is not enough. Rather, the local thermal performance of each building element (wall, roof, windows, ...) is required.

An accurate energy audit of a building therefore needs an estimation of the walls thermal transmittance U or thermal resistance R. Existing standardized methods are based on steady-state assumptions. They usually require very long measurements and are highly sensitive to outdoor conditions. Several dynamic and active methods were also developed in academia. They are usually robust to outdoor conditions. However, these methods also present some limitations which should be addressed for a wider uptake of *in situ* measurements by the construction industry. The duration required to perform *in situ* measurement is often recognized as the main challenge.

In this context, this study proposes an active methodology. It mainly consists in heating the indoor air and using inverse methods to estimate the wall thermal resistance from heat flux and temperature measurements. Unlike active temperature-temperature common approaches, this heat flux-temperature alternative enables to bypass the surface heat transfer coefficient and therefore to reduce a major source of uncertainty (problem of parameter identifiability, see [4] for instance). In addition, only a few hours of measurements (typically 6 to 8) are required. Two types of approaches are proposed for the inverse procedure. First, non-linear "white-box" models are used. They are derived from the heat equation and model the different layers of the wall. The models of the second type are linear "black-box" models from the ARX framework. The methods are validated on a full-scale wall built inside a climate chamber. The layout of this wall is commonly found in the French building stock: it is a load bearing wall with an internal insulation system.

Section 2 of this paper presents a state of the art of *in situ* measurements methods for the assessment of building wall thermal resistance (or transmittance). Section 3 presents the wall studied in the present work, its steady-state characteri-

zation and the equipment used. Section 4 details the inverse methods and the two types of models implemented: "white" and "black" box. Results on an example are detailed to illustrate the methods. Finally, the latter are tested on various conditions in section 5 to assess their robustness.

2 State of the art

Several reviews of *in situ* measurement methods of U-value were recently published (e.g., see Bienvenido-Huertas *et al.* [5], Soares *et al.* [6] and Teni *et al.* [7]).

The techniques may be classified in three categories: steady-state, dynamic and active methods. In the two last categories, the dynamic behavior of the wall is analyzed, the difference is that active methods rely on an artificial thermal load.

Steady-state methods are more commonly used because they are rather simple to implement and to analyze. In the literature, many authors refer to the two following standards: ISO 8990 [8] and ISO 9869-1 [9]. The former details the experimental protocol to use in order to measure the thermal resistance R of a wall in steady-state thanks to the use of a hot box test facility. However, the ISO 9869-1 [9] standard deals with *in situ* measurements. The method consists in implementing a heat flux meter (HFM) on the internal surface of a wall and to measure the internal and external temperatures. This is the most used method in the community. The wall U-value is calculated from time-averages of the measured quantities. Ficco *et al.* [10] studied the experimental aspects of the application of this so-called "average method" (such as the effects of measurement conditions). This technique is based on stationary boundary conditions. Yet, proper steady-states are almost never encountered *in situ* so the average method relies on averaged data as an approximation for measurements under stationary conditions. A variation of this approach (also detailed in ISO 9869-1 [9]) adds a storage effect correction but in essence it remains a semi-stationary analysis method. Several papers highlighted the limitations of the ISO 9869-1 standard, see for instance Rasooli *et al.* [11], Evangelisti *et al.* [12], Gaspar *et al.* [13] [14].

Infrared thermography (IRT) is also widely used for the assessment of building wall thermal transmittance in steady-state. Several reviews were written on the topic, such as Balaras *et al.* [15] and Kylili *et al.* [16]. The best conditions for the use of thermography are presented and discussed in Barreira *et al.* [17] and Lehmann *et al.* [18]. Passive IRT is a commonly used tool for qualitative assessments of building envelopes (see ISO 13187 [19]). It enables to detect irregularities and defaults on a building envelope (see for instance Ocaña *et al.* [20], Garcez *et al.* [21], Menezes et al [22] and Taylor *et al.* [23]). Standard ISO 9869-2 [24] describes a methodology to estimate wall thermal transmittance from passive IRT and other sensors. The method is derived from Kato *et al.* [25]. It uses specific sensors to measure the operative temperature on each side of the wall as well as the indoor total heat transfer coefficient. Many studies use a method based on the decomposition of the surface heat flux into its radiative and convective components in steady-state. Some focused on indoor measurements. Madding [26] and Tejedor *et al.* [27] [28] estimated the convective heat transfer coefficient from empirical correlations while Fokaides *et al.* [29] used values from ISO 6946 [30]. In addition, Danielski *et al.* [31] used linear regression between measured heat flux and indoor/outdoor temperature differences to estimate the wall thermal transmittance. Other studies rather focused on outdoor measurements. Albatici *et al.* [32] [33], Nardi *et al.* [34] and Dall'O *et al.* [35] used an empirical correlation based on the wind speed to estimate the heat transfer coefficient. Bienvenido *et al.* thoroughly studied the influence of the correlation chosen for the internal [36] and external [37] coefficients on results of quantitative IRT methods. Finally, Ibos *et al.* [38] implemented and compared three IRT methods to ISO 9869-1 [9] and pointed out the high dispersion results obtained. Nevertheless, for steady-state methods to be accurate, several recommendations have to be followed, which limits their applicability. For instance, the weather conditions have to remain constant during several consecutive days to ensure a quasi-steady-state regime and measurements have to last for at least several days, up to several months.

Dynamic methods were developed to overcome the limitations of steady-state approaches. Basically, more advanced dynamic data analysis include the fluctuations in measured heat fluxes and temperatures instead of canceling them out. In essence, they are models constructed from measurement data (inverse modeling). Roulet *et al.* [39] proposed a linear model having a thermal conductivity and several time constants as unknowns. The system of equation is solved using ordinary least squares (OLS) based on measurements data. Anderlind [40] [41] later proposed a simplification of this approach by expressing the heat flux as the sum of two terms: one for the steady-state behavior and the other for dynamic variations. Alternatively, many studies used stochastic gray-box models: Gutschker [42], Baker *et al.* [43], Jimenez *et al.* [44], Deconinck *et al.* [45] [46], Naveros *et al.* [47] and Bacher *et al.* [48]. Theses models depend on parameters which have a physical meaning (usually thermal resistances and capacities: the so-called R-C models). Biddulph *et al.* [49] proposed a method using Bayesian inference to estimate the parameters and this method was improved by Gori *et al.* [50] [51]. De Simon *et al.* [52] also applied Bayesian inference to quantify the estimation uncertainty of thermophysical properties of walls. Bienvenido *et al.* [53] developed a multilayer perceptron to estimate the U-value with the correction for storage effects. The authors then optimized the method [54] and compared it two other types of data processing tools [55].

Other studies use black-box ARX models ("Auto Regressive with eXogenous inputs"). ARX models (and similar models such as ARMA, ARMAX, ...) belong to the System Identification area. This framework is a well known domain that has its main application in automatic (for control purpose mainly) and in signal processing [56]. They have the advantage of being rather simple to use. Jimenez *et al.* [57] was one of the first to use ARX models for the estimation of physical parameters. The authors present the relationship between R-C networks and parametric models. Naveros *et al.* [58] further developed this idea. Several other references used ARX models and usually made a comparison with some of the above-mentioned methods: Lambie *et al.* [59] [44], Jimenez *et al.* [60], Deconinck *et al.* [45]. Madsen *et al.* [61] provided guidelines for the thermal performance characterization using time series data in buildings. Jimenez *et al.* [60] compare linear and non linear approaches. ARX models are also used for the *in situ* characterization of building global heat loss

coefficient (HLC): [62] [63] [64].

However, these models require a significant amount of data to be accurate (several days to several weeks). By using an artificial thermal load, active methods are a good alternative. Not only are they faster than other methods, they are also less sensitive to weather conditions. Gagliano *et al.* [65] and Ricciu *et al.* [66] estimated the dynamic thermal properties of walls using a harmonic thermal load, following recommendations from standard ISO 13786 [67]. The properties are estimated from an inverse technique based on the phase lag and amplitude ratio of temperature and heat flux either side of the wall. Lakatos *et al.* [68] applied the same method for the characterization of opaque aerogel insulation blankets. However, these harmonic approaches were used in climate chamber and are not very suitable for *in situ* measurements. Meulemans *et al.* [69] [70] [71] present a method which consists in heating the interior of a building and fitting a simple two-parameters model to the data in order to estimate the thermal transmittance (or thermal resistance) of a building element. The main advantage of this technique is its rapidity (only a few hours are needed, typically one night). A few references use inverse techniques to estimate wall thermal resistance from active tests. Rasooli *et al.* [11] [72] present an active method based on a triangular thermal load of the internal surface. The wall thermal resistance as well as the outer layers thermal conductivity and volumetric heat capacity are determined from inverse modeling of the Response Factors. Rouchier [73] proposes an overview of the main guidelines for a careful and optimal use of inverse techniques in buildings. The methods are illustrated on the example of a simple R-C gray-box model. Yang *et al.* [74] used a heat flux-temperature deconvolution method to estimate a wall thermal resistance from reconstruction of the unit-step response. Other studies rather used "white-box" models. These approaches are inspired from the field of non-destructive testing (NDT) [75]. Larbi Youcef *et al.* [4] developed in laboratory a device to measure wall thermal resistances from active IRT. The authors use halogen spots on the internal side to ensure a uniform radiant heating inside the device. Chaffar *et al.* [76] estimated the thermal properties of homogeneous walls by heating one face and recording the temperature of the other face using IRT. However, these later studies were limited by the high sensitivity to the heat exchange coefficient.

As a conclusion, several measurement methods for the assessment of a wall thermal resistance (or transmittance) were developed in the literature. Some of them (including the standardized techniques) are based on steady-state assumptions. They usually require very long measurements and are highly sensitive to outdoor conditions. Several dynamic and active methods were also developed but most of them still rely on long measurements. Finally, some active methods are based on temperature- temperature measurements, which makes them sensitive to the surface heat transfer coefficient. The proposed method aims at overcoming these limitations.

3 Experimental setup

3.1 Presentation

The measurements were performed on a real wall built inside a climate chamber at CEREMA in Nancy, France. The latter chamber used is $4 \times 4 \times 3$ m^3 and contains two independent modules able to control the air temperature between -30 and 30°C. The wall was built between these two modules so that a different temperature can be set between each side of the wall. The wall is 3.2 m wide and 2 m high and a small door on the right hand side was installed. It is made of concrete building blocks (see Fig 1) and a standard internal insulation system (see Fig 2). This is a very common configuration encountered in French buildings.

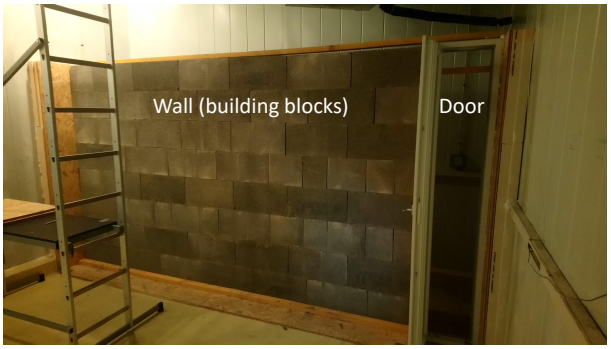

Figure 1: Photography of the wall before installation of the insulation system.

The insulation system consists in 10 cm of glass wool, gypsum plates, and some metal rails to hold them. The layout of this three-layer wall is illustrated in Fig 3. The metal rails are thermal bridges into the wall: the heat transfers are two or three dimensional in their vicinity. Yet, the gypsum plate in the middle is only attached by rails on its borders, so there is a large "sound area" (1.2 m free of thermal bridge) in the center of the wall. An infrared camera was used to check if heat transfers on this area are really 1D, that is to say if the surface temperature is uniform.

Figure 2: Photography of the wall before installation of the last gypsum boards.

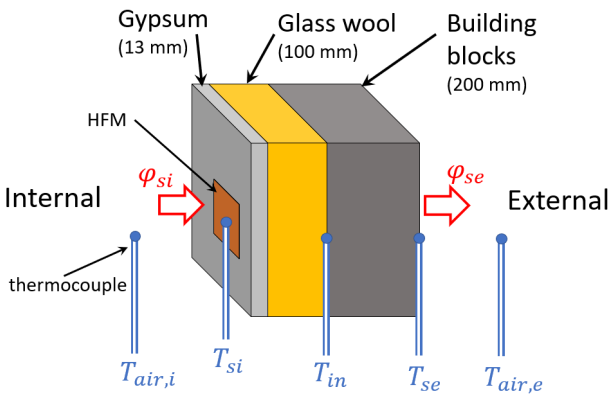

Figure 3: Scheme of the wall layout.

3.2 Sensors and data acquisition

Several contact sensors were implemented inside the climate chamber: on the wall surface as well as inside it. They are illustrated in Fig 3. Heat flux meters from the Captec© manufacturer monitor the surface heat fluxes. They are 100 × 100 mm² large, have a 0.54 mm thickness and a sensitivity superior to 60 µV.(W.m^{-2})$^{-1}$ given with a 3 % uncertainty. Temperatures are measured with type-T thermocouples. The air temperature is measured in the center of the room by thermocouples shielded from radiation with aluminum tape. A platinum sensor was used to calibrate the thermocouples over the range 0°C - 50°C. It was used with an AOIP TM6612 temperature datalogger. The measurement uncertainty of this reference is 0.2°C. An external calibration of these devices was performed in order to ensure the metrological traceability to the ITS-90 [77]. The HFMs were covered with adhesive tape that have similar optical properties as the wall surface: same emissivity (0.94 in the 2-20 µm band) and diffuse reflection[1]. This enables the sensors to be as less intrusive as possible. Temperatures and heat fluxes are recorded every 3 s and averaged every 5 points. HFMs and TCs are plugged on National Instruments© NI9214 conditioning modules. These modules communicate with a PC computer via a 8-slot NI CompactDAQ USB chassis. The experimental setup is monitored by a LabView© application.

3.3 Steady-state characterization

The thermal resistance of the wall was first determined according to ISO 9869-1 [9]. The values obtained are used as references for validation of the active methods. A 20 K temperature difference is imposed between the internal and external ambiances for several days (at least three) so that a steady-state is reached. The regulation system of the climate chamber avoids any significant air stratification. The wall thermal resistance is worked out from measurement of the surface heat flux φ_{si} (with a HFM on the sound area of the internal surface) and the temperature difference ΔT_{sie} between the two faces of the wall:

$$R = \frac{\Delta T_{sie}}{\varphi_{si}} \quad (1)$$

Similarly, the thermal resistance of the insulation system (gypsum + glass wool) was determined from measurement of the temperature between the glass wool layer and the building blocks. The values obtained are summarized in Tab 1.

Table 1: Measured quantities and calculated thermal resistance (ISO 9869-1 [9]).

	Whole wall	Insulation system (gypsum+glass wool)
ΔT_{sie} (K)	18.9 ± 0.1	16.9 ± 0.1
φ_{si} (W.m^{-2})	$5.35 \pm 3\%$	$5.35 \pm 3\%$
R (m^2.K.W^{-1})	3.49 ± 0.11	3.15 ± 0.10

The uncertainties on R are propagated from measurement uncertainties on ΔT and φ [78]:

$$u_R = R \times \sqrt{\left(\frac{u_{\Delta T}}{\Delta T}\right)^2 + \left(\frac{u_\varphi}{\varphi}\right)^2} \quad (2)$$

According to the manufacturer, the glass wool has a thermal resistance of 3.12 m^2.K^1.W^{-1} (for a 100 mm thickness). This value is in good agreement with the measured thermal resistance of the insulation system (which is slightly above because it includes the gypsum layer).

4 Dynamic (active) methodologies

This section presents the two active methods developed. There are based on the same measurement data. The algorithms used were implemented in Matlab.

4.1 Experimental protocol

4.1.1 Presentation

To perform active measurements, one needs to apply an artificial thermal load to the building. In the present study, it was chosen to use two 500 W electric fan heaters to heat up the internal air. This thermal load (which is similar to the one used in the QUB/e method [69]) has the advantage of being easy to implement *in situ*. In addition, it provides a rather uniform heating of the wall (not perfect because of air stratification). In contrast, the use of a radiant heating source would only heat up a limited area of the wall. The air temperatures measured during a typical active test are plotted in Fig 4. The initial internal and external temperatures were set at 15 and 5°C respectively for two days so that a steady-state was achieved. When the heaters are turned on, the regulation system on the same side of the wall is simultaneously turned off. After 8 hours of constant heating, the internal air temperature rises by 15°C up to 30°C. The temperature oscillations observed in Fig 4 are due to the climate chamber regulation systems.

[1] The emissivities were measured with an infrared spectrometer (Frontier model, from Perkin-Elmer©) equipped with an integrating sphere (from Pike©). A diffusing gold surface (SpectraGold©) was used as reference and its reflectance was measured by an independent method at the French National Metrology Institute (LNE: Laboratoire National de métrologie et d'Essais).

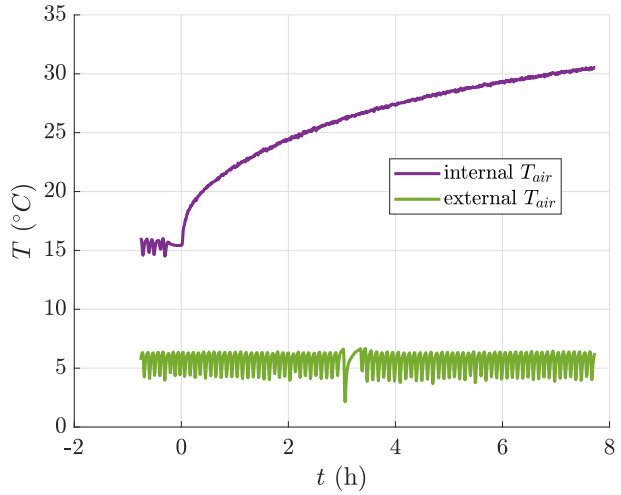

Figure 4: Internal and external air temperatures during an active test (the heaters are turned on at $t = 0$).

Figure 5 plots the evolution of the wall surface temperature T_{si} and heat flux φ_{si}, measured on the sound area (away from the thermal bridges) during the same experiment. The temperature T_{in} of the interface between the glass wool and the concrete blocks is also plotted. The surface temperature increases up to 28°C whereas the heat flux rapidly reaches a maximum and then decreases. Temperature T_{in} remains almost constant during the experiment.

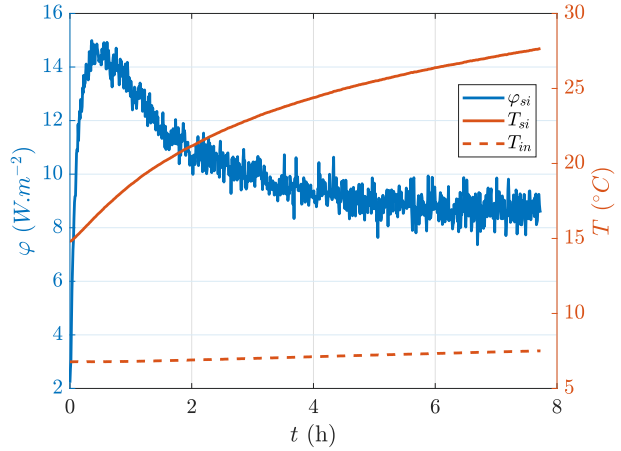

Figure 5: Surface heat flux and temperature measured on the internal wall surface during an active test, as well as wall internal temperature.

Indoor surface quantities T_{si} and φ_{si} will be fed to the models in order to work out the wall thermal resistance. Instead of φ_{si}, the indoor room temperature T_i could have been chosen. Heat flux φ_{si} was preferred for several reasons. First, a model built with T_{si} and T_i would have to include an additional parameter: the total heat transfer coefficient h. This quantity accounts for both radiative and convective heat transfers. The inverse problem (see section 4.2) would be more ill-posed because this additional parameter would have a very high sensitivity whereas its value is of no interest in our study. Second, temperature T_i is very complex to measure as it is the so called "operative temperature". Similarly to the h coefficient, it combines radiative and convective surface heat transfers. In the building sector, the operative temperature is usually supposed equal to the air temperature. This assumption is relevant in quasi-steady state, when the indoor environment is close to thermal equilibrium. However, it is no longer valid here in active tests. Because the internal air is rapidly heated, its temperature becomes very different from the mean radiant temperature. Consequently, using φ_{si} and T_{si} as inputs of the inverse model allow overcoming these difficulties.

4.1.2 Measurement campaign

To assess the repeatability and robustness of the method, several configurations were tested during the experimental campaign. There are summarized in Tab 2. During the whole campaign, the internal air temperature $T_{air,i}$ remains equal to 15°C (except of course during the active tests). The differences come from the external air temperature $T_{air,e}$. In configurations 1 and 2, the external air temperature $T_{air,e}$ is constant and equal to 5 and 15°C respectively. In these configurations, the wall is at thermal equilibrium before the test. The data plotted in figures 4 and 5 were measured in configuration 1.

In the other configurations, $T_{air,e}$ is no longer constant: it has a sinusoïdal evolution which simulates day/ night cycles. The mean value of these oscillations is 5°C except for configuration 6 (15°C). Three amplitudes were tested: 5, 10 and 15 K (peak-to-peak amplitudes) for configurations 3, 4 and 5-6 respectively.

Table 2: Summary of active tests configurations.

Config	$T_{air,i}$ (°C)	$T_{air,e}$ (°C)	number of tests
1	15	5	5
2	15	15	3
3	15	$5 + 2.5\cos(\omega t)$	4
4	15	$5 + 5.0\cos(\omega t)$	4
5	15	$5 + 7.5\cos(\omega t)$	8
6	15	$15 + 7.5\cos(\omega t)$	3

Even though the oscillations simulate day/night cycles, their period was set to 32 h instead of 24 h. This setting has a practical motivation: it enables to perform an active test every day at the same hour with different $T_{air,e}$. This is illustrated in Fig 6 where the temperatures are plotted for several consecutive days (T_{in} is the temperature of the interface between the glass wool and the concrete blocks). This simulates *in situ* experiments undertaken at different moments of the day. Given that low frequencies thermal waves penetrate deeper a wall than high frequencies ones, the chosen period of 32 h is a conservative choice.

4.2 Estimation approach 1: white-box models

This method consists in using an inverse technique with a "white-box" model to estimate the thermal properties of the

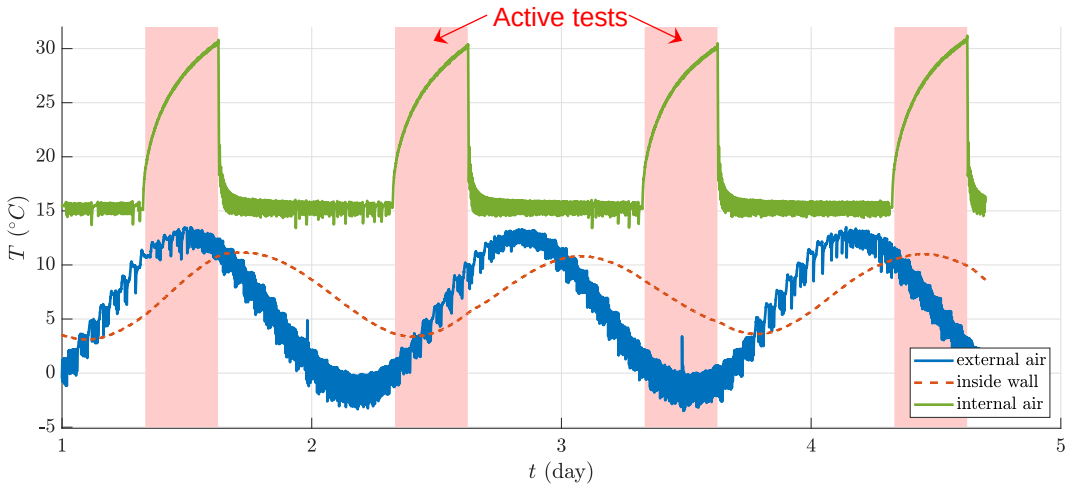

Figure 6: Example of internal and external temperatures for consecutive active tests (configuration 5).

wall from measurements. Throughout this section, one experiment is taken as an example to present the active method. It is the one already introduced in Fig 4 and it belongs to configuration 1.

4.2.1 Presentation of inverse technique used

This is a non-linear parameter estimation problem [79] [80]. First, a direct model has to be defined. In this study, the surface heat flux φ_{si} was chosen to be the output of the model whereas measured temperatures are inputs. The other way around could have been used but, as detailed below, only the noise on the output is taken into account in the analysis while the noise on the inputs has to be neglected. Given that measurement noise is much more significant on φ_{si} than T_{si} (see Fig 5), the former was chosen as output.

We define a model φ_{mo} which depends on some parameters gathered in the vector $\boldsymbol{\beta}$. It is supposed unbiased and corrupted by a Gaussian noise ε of zero mean and of standard deviation σ_φ:

$$\boldsymbol{\varphi} = \boldsymbol{\varphi}_{mo}(\boldsymbol{\beta}) + \boldsymbol{\varepsilon} \tag{3}$$

with $\boldsymbol{\varphi}$ the measurements. For the sake of clarity, the dependency to the inputs (such as T_{si}) is omitted in the notations. The objective of the inversion procedure is to find the optimum parameter vector $\widehat{\boldsymbol{\beta}}$ that minimizes the difference between the model and the measurements. This difference is quantified by the quadratic cost function J:

$$J(\boldsymbol{\beta}) = \sum_{i=1}^{N} \left(\varphi(t_i) - \varphi_{mo}(\boldsymbol{\beta}, t_i)\right)^2 \tag{4}$$

with N the number of measurement points and t the time. Because the model is non-linear in its parameter, the optimum vector $\widehat{\boldsymbol{\beta}}$ is determined by an iterative procedure (see section 4.2.5). Inverse problems are ill-posed in the Hadamard sense [81], parameters estimation by inverse methods are thus not straightforward to use. One must therefore be careful in the choice of the direct problem: its complexity has to be adapted to the problem. Indeed, a model with too few parameters will not be able to capture the physical phenomenon encountered while a model with too many parameters will be ill-posed and will not be identifiable. The model needs to have about as many parameters as degrees of freedom of the problem. Several tools are useful to determine the number of degrees of freedom, that will be presented in the next paragraphs.

4.2.2 Direct model definition and reduction

The direct model is built using the thermal quadrupole formalism [82]. This approach uses the Laplace transform of the heat equation. The thermal quadrupoles are very convenient to model one-dimensional multi-layer problems, like the current one. In the Laplace domain, the relationships between the surface temperature and heat flux on each side of the wall are simply given by a 2-by-2 matrix multiplication:

$$\begin{bmatrix} \widetilde{T_{si}} \\ \widetilde{\varphi_{si}} \end{bmatrix} = M \times \begin{bmatrix} \widetilde{T_{se}} \\ \widetilde{\varphi_{se}} \end{bmatrix} \tag{5}$$

where the coefficients of matrix M contain the intrinsic thermal properties of the wall. In the case of a single homogeneous layer k, its matrix is given by:

$$M_k = \begin{bmatrix} \cosh\left(R_k b_k \sqrt{p}\right) & \sinh\left(R_k b_k \sqrt{p}\right) / \left(b_k \sqrt{p}\right) \\ \sinh\left(R_k b_k \sqrt{p}\right) \times b_k \sqrt{p} & \cosh\left(R_k b_k \sqrt{p}\right) \end{bmatrix} \tag{6}$$

with R_k and b_k the thermal resistance and effusivity of the layer. The couple (R, b) was chosen to parameterize the quadrupole matrix because R is the parameter we want to estimate here and b has the advantage of being independent on the layer thickness. Basically, any couple of quantities among R, b, C, and τ could have been equally selected (C is the layer thermal capacity and τ its thermal characteristic time). This choice has no impact on the well-posedness of the problem: R will be estimated with the same uncertainty regardless of the other parameter chosen.

In the case of a multi-layer wall, matrix M is simply given by multiplication of each layer matrix. For a three-layer wall, matrix M is given by:

$$M = M_1 M_2 M_3 \tag{7}$$

In the present study, indices 1, 2 and 3 refer to the gypsum, glass wool and building blocks layers respectively. The contact resistance between each layer has been ignored hereby because they are much smaller than the resistance of building materials. We introduce the following notation:

$$M = \begin{bmatrix} A & B \\ C & D \end{bmatrix} \tag{8}$$

Thus, Eq 5 may be re-written as:

$$\widetilde{\varphi_{\mathrm{si}}} = \frac{D}{B}\widetilde{T_{\mathrm{si}}} + \frac{1}{B}\widetilde{T_{\mathrm{se}}} \tag{9}$$

This means that if the thermal properties of the wall are known, $\widetilde{\varphi_{\mathrm{si}}}$ can be derived from $\widetilde{T_{\mathrm{si}}}$ and $\widetilde{T_{\mathrm{se}}}$. The De Hoog algorithm [83] is finally used to numerically work out the inverse Laplace transform and generate data in the time domain.

From Eq 9, for different models (named A, B, C and D) were derived. These are presented below and summarized in Tab 3.

Model A

This model uses a simplified version of Eq 9. It has been observed that during the duration of an active experiment (typically maximum 8 h), the temperature T_{in} of the interface between the glass wool and the concrete blocks barely increases (see Fig 5). Indeed, not only are the blocks located behind an insulating material (the thermal wave needs time to reach them), they have also a very high thermal inertia. Thus, model A excludes the third layer and replaces it by the boundary condition T_{in}=constant. Since initial values are removed, this is equivalent to $\widetilde{T_{\mathrm{in}}} = 0$. This model only takes into account the first two layers (gypsum and glass wool) hence the "1-2" subscripts in Tab 3. This simplified model has four unknown parameters (two per modeled layer) and is useful to estimate the thermal resistance of the insulation system. The concrete blocks have a little contribution to the overall thermal resistance anyway.

Model B

Similarly to model A, the concrete blocks layer is excluded from model B and the same four unknown parameters remain. However, temperature T_{in} is not supposed null but is measured. Model B therefore has two inputs: T_{si} and T_{in}. This configuration is not applicable *in situ* since no thermocouple can be installed inside the wall. Nevertheless, it is useful to gain valuable insight on the experiment. In addition, in the case of a light wall (without high inertia materials), this two layers model could be applied by replacing T_{in} by T_{se}.

Model C

This model is more complete than the previous ones as it includes all three layers (see the "1-3" subscripts in Tab 3). Thus, model C has six parameters. The rear surface temperature T_{se} is measured and is an input of the model. However, the parameters of the third layer (R_3 and b_3) cannot be estimated with the other ones because of strong correlations (see section 4.2.4): they are supposed to be known. In practice, one could use standard values for this type of material. For more accuracy, it is proposed here to estimate them by using model D.

Model D

This model differs from the others as it is not meant to estimate the thermal resistance of the insulation system. It was built to provide values of R_3 and b_3 to feed model C and only models the building blocks ("3" subscript). It takes as output the surface heat flux φ_{se} measured with a HFM on the external side of the wall. The input is the external surface temperature T_{se}. As boundary condition, the heat flux between layers 2 and 3 is supposed null. This simplifying assumption is deemed reasonable given the presence of thermal insulation. This model is not applicable if the external temperature is constant. It can therefore only be used in configurations 3 to 6.

4.2.3 Implementation of model inputs

The direct models depend on the parameter vector $\boldsymbol{\beta}$ but also on one or two inputs (see equations in Tab 3). These inputs are temperatures: T_{si}, T_{in} or T_{se}. The thermal quadrupole formalism requires to have an analytical expression of the Laplace transform of these temperatures (see Eq 9). In Non Destructive Testing [75], thermal loads are usually a pulse or a step, so that the Laplace transform of the input is simple and only depends on one constant. Here, the evolution of the inputs is more complex. Therefore, the chosen approach is to fit a function of known Laplace transform on the input curves. This function does not need to have any physical meaning, but is must be as close as possible to the measured data. Several functions were tested and it was found that a polynomial fitted well T_{in} or T_{se} whereas a polynomial in $1/j$ gave better results on T_{si}:

$$T_{\mathrm{si}}(\boldsymbol{\alpha}, t) = \sum_{j=1}^{m} \alpha_j t^{1/j} \tag{10}$$

with $\boldsymbol{\alpha}$ the vector of parameters that is adjusted during the fitting process. The later is made with the Levenberg-Marquardt algorithm (see paragraph 4.2.5). The Laplace transform of the previous function is given by:

$$\widetilde{T_{\mathrm{si}}}(\boldsymbol{\alpha}, p) = \sum_{j=1}^{m} \alpha_j \frac{\Gamma\left(\frac{1}{j}+1\right)}{p^{\frac{1}{j}+1}} \tag{11}$$

with Γ the gamma function. Figure 7 shows the fit on the example of T_{si} with $m = 7$. It may be seen that the chosen function fits well the measurement data. The degree m of the polynomial was set high enough to make the residuals (difference between measurements and model) as low as possible. A high degree do not affect the well-posedness of the problem, it only lightly slows down the calculations (which is not an issue given that the estimation is almost instantaneous).

The components of vector $\boldsymbol{\alpha}$ are set before estimation of the thermal resistance so they are not included in the vector of unknown parameters $\boldsymbol{\beta}$. In addition, it is important to point out that this fit removes the measurement noise on the inputs of models A, B, C and D (see Tab 3). Therefore, this noise will be supposed null in the evaluation of the estimation uncertainties of the wall thermal resistance: only the noise on the output φ_{si} is taken into account (see next paragraph). Yet, given that the signal to noise ratio is a great deal higher on the temperatures than on the heat flux, this hypothesis

Table 3: Summary of "white-box" direct models.

Model	Illustration	Equation	Parameters
A	φ_{si}, T_{si}, 1, 2, $T_{in} = cst$	$\widetilde{\varphi_{\mathrm{si}}} = \frac{D_{1-2}}{B_{1-2}}\widetilde{T_{\mathrm{si}}}$	$\boldsymbol{\beta} = [R_1 \;\; b_1 \;\; R_2 \;\; b_2]$
B	φ_{si}, T_{si}, 1, 2, T_{in}	$\widetilde{\varphi_{\mathrm{si}}} = \frac{D_{1-2}}{B_{1-2}}\widetilde{T_{\mathrm{si}}} + \frac{1}{B_{1-2}}\widetilde{T_{\mathrm{in}}}$	$\boldsymbol{\beta} = [R_1 \;\; b_1 \;\; R_2 \;\; b_2]$
C	φ_{si}, T_{si}, 1, 2, 3, T_{se}	$\widetilde{\varphi_{\mathrm{si}}} = \frac{D_{1-3}}{B_{1-3}}\widetilde{T_{\mathrm{si}}} + \frac{1}{B_{1-3}}\widetilde{T_{\mathrm{se}}}$	$\boldsymbol{\beta} = [R_1 \;\; b_1 \;\; R_2 \;\; b_2 \;\; R_3 \;\; b_3]$ (R_3 and b_3 are supposed to be known)
D	$\varphi_{in} = 0$, 3, φ_{se}, T_{se}	$\widetilde{\varphi_{\mathrm{se}}} = \frac{C_3}{A_3}\widetilde{T_{\mathrm{se}}}$	$\boldsymbol{\beta} = [R_3 \;\; b_3]$

has a limited impact on the uncertainty calculation. This justifies the choice of φ_{si} as output.

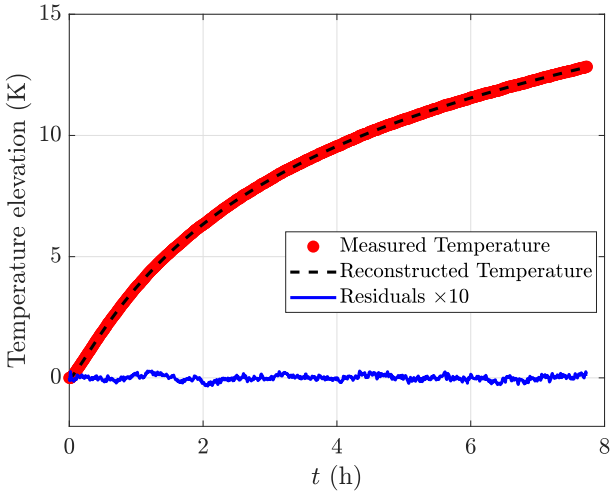

Figure 7: Polynomial fit on model input T_{si} (with $m = 7$).

4.2.4 Sensitivity analysis and estimation uncertainties

Inverse problems are usually ill-posed. The sensitivity analysis is required to determine the model number of degrees of freedom and to assess the identifiability of the parameters. For the sake of conciseness, only the sensitivity analysis of model A is detailed here.

We define the reduced sensitivity coefficients to each parameter β_j:

$$\boldsymbol{X}^*(\beta_j) = \beta_j \frac{\partial \boldsymbol{\varphi}_{\mathrm{mo}}}{\partial \beta_j} \tag{12}$$

These coefficients are all expressed in the unit of the output which makes them comparable. In non-linear problems such as this one, sensitivities are defined locally (they depend on $\boldsymbol{\beta}$). Figure 8 plots the evolution of these sensitivities with $\boldsymbol{\beta} = \widehat{\boldsymbol{\beta}}$ the optimum vector after parameter estimation (see section 4.2.5).

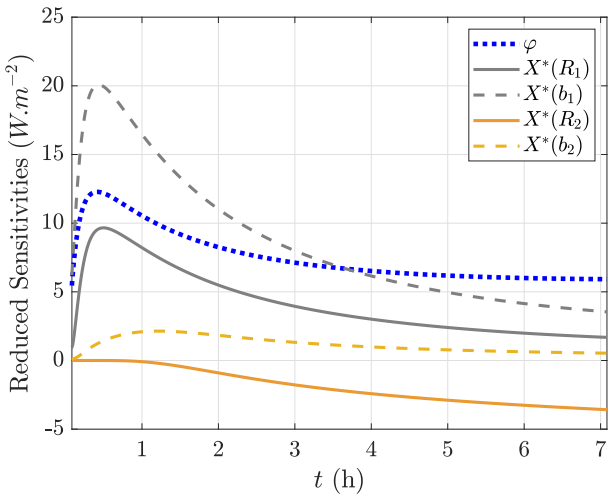

Figure 8: Reduced sensitivities of model A (configuration 1).

First, it may be noted that the sensitivities to the parameters of the first layer, R_1 and b_1 have a larger amplitude than those of the second layer (R_2 and b_2). This is because the model is more sensitive to parameters of the closest layer to the measurement location of φ_{si}. The curves of $X^*(R_1)$ and $X^*(b_1)$ also have a similar shape: R_1 and b_1 are correlated. It might be complex to estimate them both accurately: many different combinations of them might predict the same heat flux φ_{mo}. In addition, b_2 has a low reduced sensitivity when compared to the other ones so its estimation uncertainty will be greater. Finally, the sensitivity to R_2 has a non negligible

amplitude and a unique shape.

The sensitivity to R_2 keeps increasing with time (in absolute values). This suggests that there is a minimum experiment duration for the estimation of R_2 to be accurate. In addition, because the sensitivity to R_2 is small at the beginning of the experiment, the first instants are not taken into account in the estimation procedure.

The uncertainty over the estimated parameters are derived from the variance-covariance matrix:

$$cov \approx \begin{bmatrix} \text{var}\left(\hat{\beta}_i\right) & \text{cov}\left(\hat{\beta}_i, \hat{\beta}_j\right) & \cdots \\ \text{cov}\left(\hat{\beta}_i, \hat{\beta}_j\right) & \text{var}\left(\hat{\beta}_j\right) & \cdots \\ \vdots & \vdots & \ddots \end{bmatrix} \tag{13}$$

with

$$cov = \sigma_\varphi^2 \left(X^T X\right)^{-1} \tag{14}$$

Thus, the variances over the estimated parameters are directly proportional to the variance σ_φ^2 of the heat flux measurement noise. If the measurement uncertainty includes a constant component (bias), this one is removed when the initial conditions are subtracted. This is one of the advantages of the active approach: only variations in temperatures and heat fluxes are analyzed.

We define the hybrid matrix V_{cor}:

$$V_{\text{cor}} \approx \begin{bmatrix} \sqrt{\text{var}\left(\hat{\beta}_i\right)}/\hat{\beta}_i & \rho_{ij} & \cdots \\ \rho_{ij} & \sqrt{\text{var}\left(\hat{\beta}_j\right)}/\hat{\beta}_j & \cdots \\ \vdots & \vdots & \ddots \end{bmatrix} \tag{15}$$

where the off-diagonal terms are the correlation parameters. They range between -1 and 1 and quantify the correlations between pairs of parameters: the closer ρ_{ij} is to -1 or 1, the more parameters β_i and β_j are correlated. The diagonal terms of the V_{cor} matrix are the relative uncertainty of estimation of the parameters. The matrix is symmetric. For the given example (Fig 5):

$$V_{\text{cor}} = \begin{bmatrix} 0.13 & 0.98 & -0.31 & -0.67 \\ & 0.06 & 0.26 & 0.53 \\ & & 0.02 & 0.52 \\ \text{sym} & & & 0.10 \end{bmatrix} \tag{16}$$

where the noise level taken was representative of an experiment: $\sigma_\varphi = 0.4$ W.m^{-2}. In addition, reference values for the parameter were taken. They are given in Tab 4.

The comments previously made on Fig 8 are confirmed by this matrix. Indeed, the correlation coefficient between R_1 and b_1 is close to 1 (-0.98) which proves that these two parameters are correlated. Also, parameter b_2 is estimated with a relative uncertainty of 10% whereas it is not very much correlated to any other parameter. This is due to its low sensitivity. The estimation of R_2 is rather accurate given that its relative uncertainty is only 2%.

4.2.5 Parameter estimation

The optimum parameter vector $\widehat{\boldsymbol{\beta}}$ that minimizes the distance between the model and the measurements is estimated using the Levenberg-Marquardt algorithm described in [84], [85] and [86]. This algorithm is commonly used in parameter estimation problems because of its robustness. Figure 9 plots the measurement data φ_{si} alongside the reconstructed model after estimation of the optimum parameters. The latter are given in Tab 4. The residuals are unsigned (flat) and of rather small magnitude, which is a prerequisite for the parameter estimation to be accurate.

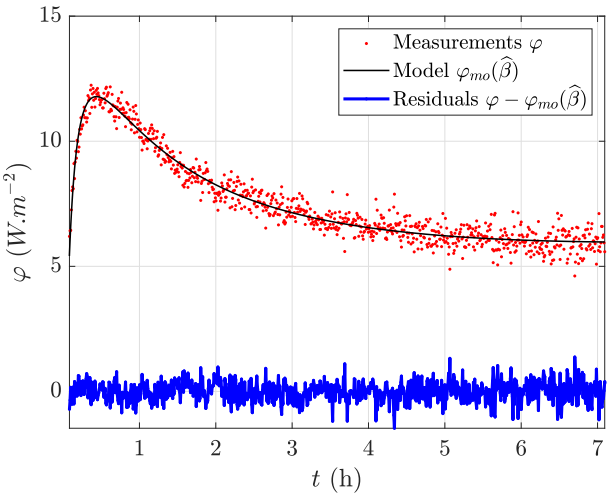

Figure 9: Comparison between measurements and reconstructed model after parameter estimation.

Table 4: Estimated parameters $\widehat{\boldsymbol{\beta}}$ with reference values.

$\widehat{\boldsymbol{\beta}}$	unit	estimation	reference
R_1	m^2.K.W^{-1}	0.05 ± 0.01	0.06
b_1	J.K^{-1}.m^{-2}.s$^{-1/2}$	421 ± 24	420
R_2	m^2.K.W^{-1}	3.04 ± 0.05	3.12
b_2	J.K^{-1}.m^{-2}.s$^{-1/2}$	35.9 ± 3.5	2

The reference values given in Tab 4 have different origins: measurements in laboratory with the Hot Disk method [87] (for R_1 and b_1), manufacturer data (for R_2) and standard value from the literature [88] ($b_2 = 21$ J.K^{-1}.m^{-2}.s$^{-1/2}$, calculated from thermal conductivity and diffusivity).

Thus, the proposed inverse method successfully estimated the thermal properties of the insulation system, especially R_1, b_1 and R_2. Thermal resistance R_2 is only about 5% away from its reference value. The estimated parameter b_2 is further from its reference value but the latter is not very much reliable because it is a standard value from the literature.

4.2.6 Robustness of the method

On the one hand, since the minimization procedure is iterative, the initial parameter vector chosen might have an impact on the estimated values if local minima of the cost function exist. It was checked here that changing the initial conditions do not affect the estimation.

On the other hand, the duration of the active tests was set to about 8 h. This choice is justified because a longer experiment would not improve the estimation of the thermal resistance. Indeed, Fig 10 plots $\widehat{R_1} + \widehat{R_2}$ and its uncertainty

for several durations of the same experiment. Only the upper limit of the time horizon is modified: the lower one is kept constant equal to 10 min. Indeed, the first points were to be removed because HFM measurements are not accurate at the beginning of the experiment (the heat flux increase is too fast). It was noted that increasing further the lower bound of the time horizon has a little impact on the results.

It may be observed on Fig 10 that after about 6 h, the estimation of the thermal resistance is no longer affected by the duration of the experiment. Also, the uncertainty on the resistance decreases during the first six hours and then stabilizes. Thus, for this wall, longer experiments are not required.

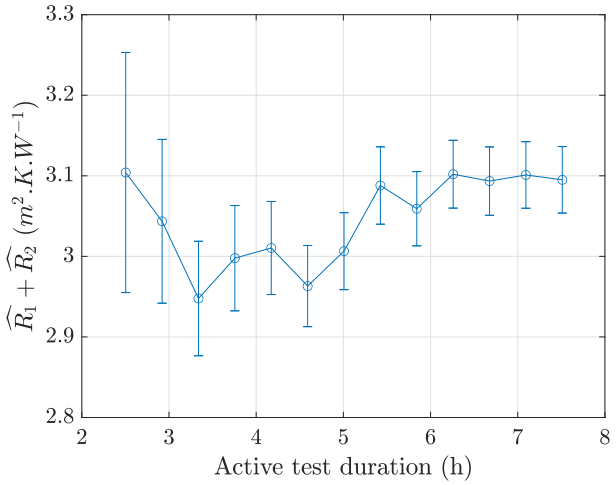

Figure 10: Impact of experiment duration (upper limit of time horizon) on thermal resistance estimation with the "white-box" approach.

4.3 Estimation approach 2: black-box models

4.3.1 Introduction to ARX models

ARX models belong to the system identification framework [56]. They consist in identifying the parameters involved in a linear relation between input(s) and output(s), from measurements of these quantities. Similarly to the "white-box" method, we take heat flux φ_{si} as input and temperatures (T_{si}, T_{in} or T_{se}) as outputs. For any point of the time series, the last few measurements points of the output are linked to the few last points of the inputs. The problem is written as:

$$A\left(q\right)\varphi_{\text{si}} = B\left(q\right)T_{\text{si}} + C\left(q\right)T_{\text{se}} \tag{17}$$

where q is the delay (or back-shift) operator defined such that $q^{-1}y\left(k\right) = y\left(k-1\right)$ with y either an input or an output time series. A, B and C are polynomials in q. Their orders are n_a, $n_b - 1$ and $n_c - 1$ respectively:

$$A\left(q\right) = 1 + a_1 q^{-1} + ... + a_{n_a} q^{-n_a} \tag{18}$$

$$B\left(q\right) = b_0 + b_1 q^{-1} + ... + b_{n_b-1} q^{-n_b+1} \tag{19}$$

$$C\left(q\right) = c_0 + c_1 q^{-1} + ... + c_{n_c-1} q^{-n_c+1} \tag{20}$$

Equation 17 is analogous to Eq 9 but parameters a_i, b_i and c_i have no physical meaning ("Black-box" model). Equations 18 to 20 define an ARMA model (Auto-Regressive with Moving Average). The ARX formulation is similar except that polynomials B and C are multiplied by a time shift operator q^{-n_k} where the number n_k is the number of input samples that occur before the input affects the output (also called the "dead time" in the system). For the sake of clarity, we take $n_k = 0$ in the following equations.

By analogy to "white-box" models A, B and C presented in Tab 3, we define three ARX models: A', B', and C'. They use the same data as their "white-box" counterparts. They are presented in Tab 5.

4.3.2 Presentation

For the sake of clarity, the methodology is detailed on the case of model A'. It only has one input (T_{si}): it is a "Single Input, Single Output" (SISO) case:

$$A\left(q\right)\varphi_{\text{si}} = B\left(q\right)T_{\text{si}} \tag{21}$$

For any instant k, an estimator of the output $\widehat{\varphi}\left(k\right)$ is given by:

$$\widehat{\varphi}\left(k\right) = -\sum_{j=1}^{n_a} a_j \varphi_{\text{si}}\left(k-j\right) + \sum_{j=0}^{n_b-1} b_j T_{\text{si}}\left(k-j\right) \tag{22}$$

The problem is linear and may be written in matrix form:

$$\boldsymbol{\varphi}_{\text{mo}}\left(\boldsymbol{\theta}\right) = H\boldsymbol{\theta} \tag{23}$$

with $\boldsymbol{\theta}$ the parameter vector:

$$\boldsymbol{\theta} = \left[a_1, ..., a_{n_a}, b_0, ..., b_{n_b-1}\right]^{\text{T}} \tag{24}$$

Matrix H contains the measured inputs and output, as shown in Eq 25 (subscripts "si" were removed for clarity):

$$H = \begin{bmatrix} \varphi\left(n-1\right) & \varphi\left(n-2\right) & \cdots & \varphi\left(n-n_a\right) & T\left(n\right) & T\left(n-1\right) & \cdots & T\left(n-n_b+1\right) \\ \varphi\left(n\right) & \varphi\left(n-1\right) & \ddots & \vdots & T\left(n+1\right) & T\left(n\right) & \ddots & \vdots \\ \vdots & \ddots & \ddots & \varphi\left(n-2\right) & \vdots & \ddots & \ddots & T\left(n-1\right) \\ \varphi\left(n+n_a-1\right) & \cdots & \varphi\left(n\right) & \varphi\left(n-1\right) & T\left(n+n_b+1\right) & \cdots & T\left(n+1\right) & T\left(n\right) \\ \vdots & \vdots & \ddots & \vdots & \vdots & \vdots & \ddots & \vdots \\ \varphi\left(N-1\right) & \varphi\left(N-2\right) & \cdots & \varphi\left(N-n_a\right) & T\left(N\right) & T\left(N-1\right) & \cdots & T\left(N-n_b+1\right) \end{bmatrix} \tag{25}$$

Table 5: Summary of ARX models.

Model	Illustration	Equation	Parameters
A'		$A(q)\,\varphi_{\mathrm{si}} = B(q)\,T_{\mathrm{si}}$	$\boldsymbol{\theta} = [a_1, ..., a_{n_a}, b_0, ..., b_{n_b-1}]$
B'	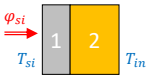	$A(q)\,\varphi_{\mathrm{si}} = B(q)\,T_{\mathrm{si}} + C(q)\,T_{\mathrm{in}}$	$\boldsymbol{\theta} = [a_1, ..., a_{n_a}, b_0, ..., b_{n_b-1}, c_0, ..., c_{n_c-1}]$
C'	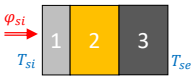	$A(q)\,\varphi_{\mathrm{si}} = B(q)\,T_{\mathrm{si}} + C(q)\,T_{\mathrm{se}}$	$\boldsymbol{\theta} = [a_1, ..., a_{n_a}, b_0, ..., b_{n_b-1}, c_0, ..., c_{n_c-1}]$

Like in the previous method (see Eq 3), the output φ_{si} is supposed corrupted with a white noise $\boldsymbol{\varepsilon}$ of standard deviation σ_φ:

$$\boldsymbol{\varphi}_{\mathrm{si}} = \boldsymbol{\varphi}_{\mathrm{mo}}(\boldsymbol{\theta}) + \boldsymbol{\varepsilon} = H\boldsymbol{\theta} + \boldsymbol{\varepsilon} \tag{26}$$

For matrix H to be full, the first $n-1$ of the N measurements points are removed:

$$\boldsymbol{\varphi}_{\mathrm{si}} = [\varphi_{\mathrm{si}}(n), \varphi_{\mathrm{si}}(n+1), ..., \varphi_{\mathrm{si}}(N)]^{\mathrm{T}} \tag{27}$$

with $n = \max(n_a + 1, n_b)$. The Ordinary Least Square (OLS) estimator $\widehat{\boldsymbol{\theta}}$ of this linear over-determined problem is:

$$\widehat{\boldsymbol{\theta}} = \left(H^{\mathrm{T}}H\right)^{-1} H^{\mathrm{T}}\boldsymbol{\varphi}_{\mathrm{si}} \tag{28}$$

We are not interested here in the values of each parameter contained in vector $\widehat{\boldsymbol{\theta}}$. However, the wall thermal resistance may be expressed explicitly in terms of these parameters. Eq 21 may be re-written into the form of a transfer function (here an admittance):

$$Y(q) = \frac{B(q)}{A(q)} = \frac{\sum_{j=0}^{n_b-1} b_j q^{-j}}{\sum_{j=0}^{n_a} a_j q^{-j}} \tag{29}$$

The thermal resistance is defined in steady-state. It is the inverse of value of the transfer function for a null frequency:

$$\widehat{R} = \frac{A(1)}{B(1)} = \frac{1 + \sum_{j=1}^{n_a} a_j}{\sum_{j=0}^{n_b-1} b_j} \tag{30}$$

4.3.3 Uncertainties

Similarly to Eq 14, the uncertainties over the parameters are given by the variance-covariance matrix:

$$cov\left(\widehat{\boldsymbol{\theta}}\right) = \sigma_\varphi^2 \left(H^{\mathrm{T}}H\right)^{-1} \tag{31}$$

These uncertainties are then propagated through Eq 30 to work out the uncertainty on R:

$$\sigma_R^2 = X.\mathrm{cov}\left(\widehat{\boldsymbol{\theta}}\right).X^{\mathrm{T}} \tag{32}$$

with X the sensitivity matrix:

$$X = \left[\frac{\partial R}{\partial a_1}, \ldots, \frac{\partial R}{\partial a_{n_a}}, \frac{\partial R}{\partial b_0}, \ldots, \frac{\partial R}{\partial b_{n_b-1}}\right] \tag{33}$$

The partial derivatives in the expression of X are then given by:

$$\begin{cases} \forall j \in [\![1; n_a]\!], & \frac{\partial R}{\partial a_j} = -\frac{A(1)}{B(1)^2} \\ \forall j \in [\![0; n_b - 1]\!], & \frac{\partial R}{\partial b_j} = \frac{1}{B(1)} \end{cases} \tag{34}$$

4.3.4 MISO case

In the MISO case (Multiple Inputs, Single Output), such as with models B' and C', there is no explicit formulation of the wall thermal resistance from parameters a_j, b_j and c_j. Instead, two thermal resistances (noted R_{i} and R_{e}) may be derived from Eq 17:

$$\widehat{R_{\mathrm{i}}} = \frac{A(1)}{B(1)} \tag{35}$$

$$\widehat{R_{\mathrm{e}}} = \frac{A(1)}{C(1)} \tag{36}$$

There is no relationship between these estimated resistances and the wall thermal resistances R_1, R_2 and R_3.

In most studies dealing with this issue, these two estimations of R are combined into a single value by a Lagrange weighting [57] [59] [62] [45]:

$$\widehat{R} = \lambda\widehat{R_{\mathrm{i}}} + (1-\lambda)\,\widehat{R_{\mathrm{e}}} \tag{37}$$

where the weighting factor λ was chosen to minimize the uncertainty on R:

$$\lambda = \frac{\mathrm{Var}(R_{\mathrm{e}}) - \mathrm{Covar}(R_{\mathrm{i}}, R_{\mathrm{e}})}{\mathrm{Var}(R_{\mathrm{i}}) + \mathrm{Var}(R_{\mathrm{e}}) - \mathrm{Covar}(R_{\mathrm{i}}, R_{\mathrm{e}})} \tag{38}$$

This formulation has no physical meaning. This procedure was tested but it turned out that the estimated value was very far from the reference and the associated uncertainty was very large. In addition, the algorithm is not stable: slightly changing the time horizon significantly changes the result. It is thought that the MISO formulation needs more data to converge than the SISO one because it has more parameters to determine. Indeed, the previous studies which successfully use this kind of MISO ARX models are all based on much longer measurement campaigns. Jiménez *et al.* [57] and Senave *et al.* [62] both used measurements recorded during 20 consecutive days to estimate a wall thermal resistance

and a HLC respectively. Lambie and Saelens [59] performed two experimental campaigns of 15 and 35 days respectivley (HLC estimation). Deconinck and Roels [45] used a dataset of 60 days and showed that a minimum of 20 days was required for their ARX method to give accurate results (thermal resistance estimation). In comparison to these durations, the present study deals with only 8 consecutive hours of measurement data which is almost two orders or magnitude shorter. From this perspective, implementing this model on more data (much longer experiments) might give better results but the present rapid method focuses on short measurements (i.e., less than 24 hours).

4.3.5 Choice of number of parameters

Number n_a, n_b and n_k (as well as n_c if applicable) have to be defined. First, it was observed that increasing n_k does not significantly change the estimated value whereas it increases notably its uncertainties. In addition, there is no physical justification here to support the existence of dead time between internal surface temperatures and heat fluxes. Therefore, n_k was set to zero. Fig 11 plots the estimated resistance $\widehat{R}$ as a function of n_a with $n_b = n_a$ for model A' and configuration 1. It may be observed than the fewer the parameters, the higher the bias on the estimated value and the higher the estimation uncertainty. To be more specific, above about $n_a = n_b = 10$, the estimated resistance and its uncertainty are both independent on the number of parameters. Thus, given that the calculations are almost instantaneous (even for a high number of parameters), setting high values for n_a and n_b is a relevant conservative choice. The $n_a = n_b$ condition was taken to simplify the analysis. It was observed that setting different values for n_a and n_b does not reduce the minimum number of parameters required for the estimation to be accurate. Consequently, $n_a = n_b = 25$ is set for the estimations.

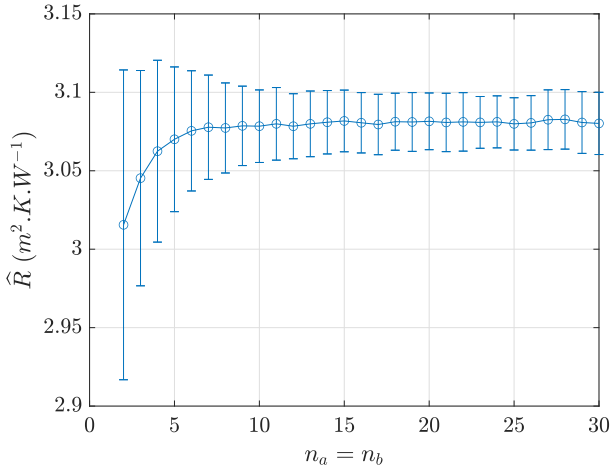

Figure 11: Impact of ARX model number of parameters on the estimated thermal resistance.

4.3.6 Impact of time horizon

Figure 12 plots the estimated thermal resistance for several durations of the active test: the time horizon upper bound is changed whereas its lower bound is kept constant (10 min). This analysis was performed on a longer test (about 12h).

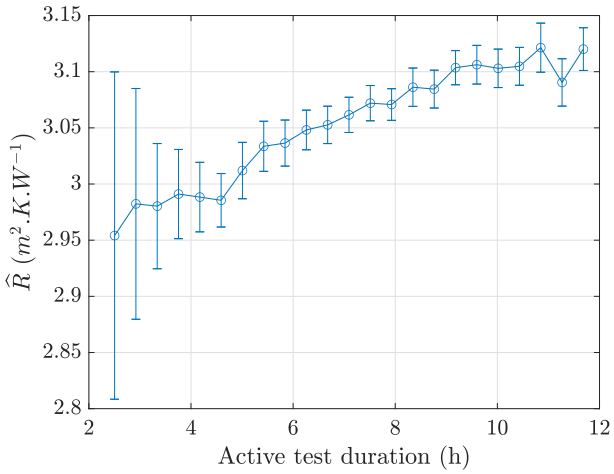

Figure 12: Impact of experiment duration on thermal resistance estimation (ARX approach).

It is clear that the uncertainty increases if the experiment duration decreases below 5 h. However, unlike with the "white-box" model (Fig 10), the estimated resistance keeps increasing slightly with time above 5 h (although the slope flattens so much that $\widehat{R}$ seems to converge after about 10h). This is because the thermal resistance $\widehat{R}$ estimated by the ARX approach is supposed to be the total resistance of the wall ($R_1 + R_2 + R_3$). In theory, $\widehat{R}$ asymptotically reaches this overall resistance after a very long time. This was checked on synthetic data modeling a much longer active test. As mentioned above, a test duration of a few hours (even 12 h) is not enough to probe the bearing layer and to estimate its thermal resistance with an active methodology. Therefore, $\widehat{R}$ corresponds here to the resistance of the insulation system.

Finally, it is interesting to point out that the ARX approach is more robust than the "white-box" approach for short experiments. Indeed, after only 2 h, it is able to estimate a thermal resistance rather close to the one of the insulation system, and with a decent uncertainty.

5 Test of the method on different configurations

5.1 Constant external conditions

This section presents the results obtained on experiments carried out when the external temperature is constant (configurations 1 and 2 in Tab 2). The thermal resistance of the insulation system (gypsum + glass wool) and the entire wall was determined using models A and A' respectively (see Tab 5). The results of estimations are summarized in Tab 6. Steady-state value are obtained from ISO 9869-1, see section 3.3. The average and standard deviation of the estimated quantities are given.

Several conclusions may be drawn from it. First, the "white-box" and "black-box" approaches give very similar results. The thermal resistance is slightly underestimated but

the distance to the reference value of R_1+R_2 is almost always below 5%. The "white-box" model seems to predict a slightly higher thermal resistance than the ARX model. Thus, both approaches estimates rather well the thermal resistance of the insulation system. It may be noted that the ARX approach was supposed to estimate the global thermal resistance of the wall: $R_1 + R_2 + R_3$. This bias is also explained by the very high thermal inertia of the building blocks layer: the latter is not probed by the active experiment.

Also, configurations 1 and 2 lead to the same results whereas they have a different initial temperature gradient: 10 and 0 K respectively. This reflects the superimposition theorem: constant temperature gradients are canceled out when initial conditions are subtracted. This is one of the main advantages of these active methods: only temperature and heat flux relative variations are analyzed. This would allow performing measurements all year long (as long as the external temperature is close to be constant), rather that only in winter like with steady-state methods.

Finally, the methods are repeatable as the dispersion of the results for the eight experiments undertaken is rather small (around 5%). It is also of the same order of magnitude as the estimation uncertainty.

Consequently, in the favorable case when the external temperature is constant, there is no need here to use more complex models to estimate the performance of the thermal insulation. Only two measured quantities are required: the internal surface heat flux φ_{si} and temperature T_{si}.

Table 6: Estimations of thermal resistance for a constant external temperature with two approaches: model A = "white-box", model A' = "black-box".

Config	Exp	Model A ($R_1 + R_2$)	Model A' ($R_1 + R_2 + R_3$)
Reference	Steady -state	3.15 ± 0.10	3.49 ± 0.11
1	1	3.09 ± 0.04	3.01 ± 0.03
	2	3.05 ± 0.03	3.01 ± 0.02
	3	3.16 ± 0.03	3.07 ± 0.02
	4	3.14 ± 0.06	2.96 ± 0.03
	5	3.07 ± 0.02	3.01 ± 0.01
2	6	3.06 ± 0.04	2.93 ± 0.02
	7	3.16 ± 0.02	3.10 ± 0.01
	8	3.09 ± 0.02	3.04 ± 0.02
average		3.10	3.01
standard deviation		0.04	0.06

It is not possible to determine the thermal resistance of the concrete layer in this configuration. Indeed, as explained above, during the 8 hours of the experiment, the temperature of the concrete blocks barely increases so this layer cannot be probed. A very much longer experiment would be required which would not be representative of *in situ* active measurements. The authors do not see it as an issue. Indeed, the bearing layer only represents a small part of the overall thermal resistance (10% here). Besides, in the context of the energy audit of a new building, the main objective it to assess the performance of the insulating materials. Finally, the method could be applied before and after energy retrofitting work to quantify the increment in thermal resistance.

5.2 Varying external conditions

When the external temperature is not stable, the estimation of the thermal resistance is more complex. This section analyzes the impact of variations in the external temperature on estimation procedures. Here, the white-box approach was used. Indeed, the ARX MISO models was not able to accurately predict the thermal resistance. The result was significantly biased and the estimation uncertainty was very large, as detailed in section 4.3.4.

Table 7 summarizes the estimations of $R_1 + R_2$ in configurations 3 to 6 using models A, B and C.

First, it may be observed that in configuration 3, the estimations only have a small bias (maximum 15%). Consequently, for this type of wall, model A is suitable when the external temperature varies with an amplitude up to about 5 K.

Then, it appears that results from model A are significantly biased for some experiments but rather accurate for others. This entirely depends on the behavior of $T_{air,e}$ before and during the experiment. In every configuration (except number 6), at least four active tests are performed following the pattern shown in Fig 6. For the first test, $T_{air,e}$ is around the maximum of its sinusoid. It increases during the second test, is around its minimum during the third one and decreases for the fourth test. These four regimes correspond to the four symbols $\cap$, $\nearrow$, $\cup$ and $\searrow$ used in Tab 7. For every configuration, model A always over-predicts the resistance when $T_{air,e}$ is around its maximum, under-predicts it when $T_{air,e}$ is around its minimum and paradoxically predicts it well when $T_{air,e}$ varies significantly. These observations are explained by the evolution of the temperature T_{in} between the insulation system and the concrete blocks (see Fig 6). Indeed, material inertia induce a phase lag of about 6 h between $T_{air,e}$ and T_{in}. Consequently, when $T_{air,e}$ is rather stable around an extremum, T_{in} varies a lot, and vice versa. Thus, inaccurate estimations correspond to situations in which T_{in} varies significantly. Model A was indeed based on the assumption of a constant T_{in}. For *in situ* applications on this type of wall, it is therefore recommended to start the active test at sunset (when the temperature starts decreasing). This is in accordance with usual guidelines for *in situ* thermal diagnoses of buildings which recommend measurements to be performed by night. The estimation uncertainties are smaller that the spread (standard deviation) between measurements, which confirms that a single experiment might lead to an accurate estimation of the thermal resistance.

Models B was developed to overcome this limitation. Instead of considering T_{in} constant, this temperature is measured and taken as an input of the model. As shown in Tab 7, the thermal resistance is now well estimated for every experiments: results are within the 10% band (relative difference to the reference value) and even within the 5% band most of the time. Hence, model B is not limited by variations of the external temperature. However, it requires to implement a temperature sensor inside the wall, which is not possible *in situ*. For a lightweight wall without significant thermal mass, the external surface temperature could be used instead.

Model C is more applicable as it only relies on surface measurements. Nevertheless, it requires prior knowledge of

Table 7: Estimations of thermal resistance for varying external temperature (cells are filled in gray when the estimated value is more than 10% away from the steady-state reference value). Depending on the experiment, $T_{\text{air,e}}$ is around a maximum: $\cap$, or increasing: $\nearrow$, or around a minimum: $\cup$, or decreasing: $\searrow$

Config	Exp	$T_{\text{air,e}}$	Model A $(R_1 + R_2)$	Model B $(R_1 + R_2)$	Model C $(R_1 + R_2)$
Reference	Steady -state	-	3.15 ± 0.10	3.15 ± 0.10	3.15 ± 0.10
3	1	$\cap$	3.62 ± 0.07	3.01 ± 0.06	2.98 ± 0.06
	2	$\nearrow$	3.20 ± 0.06	3.05 ± 0.07	3.02 ± 0.07
	3	$\cup$	2.81 ± 0.06	2.99 ± 0.07	3.01 ± 0.07
	4	$\searrow$	3.11 ± 0.05	3.02 ± 0.05	3.05 ± 0.05
4	5	$\cap$	4.19 ± 0.12	2.96 ± 0.07	2.90 ± 0.08
	6	$\nearrow$	3.25 ± 0.07	3.05 ± 0.09	3.01 ± 0.83
	7	$\cup$	2.64 ± 0.04	3.16 ± 0.05	3.20 ± 0.06
	8	$\searrow$	3.01 ± 0.05	2.93 ± 0.04	2.95 ± 0.04
5	9	$\cap$	5.84 ± 0.33	3.42 ± 0.15	3.33 ± 0.15
	10	$\cap$	6.09 ± 0.32	3.40 ± 0.13	3.36 ± 0.13
	11	$\nearrow$	3.20 ± 0.08	3.08 ± 0.10	3.06 ± 0.13
	12	$\nearrow$	3.10 ± 0.07	2.96 ± 0.09	2.93 ± 0.13
	13	$\cup$	2.23 ± 0.04	2.95 ± 0.06	2.99 ± 0.06
	14	$\cup$	2.23 ± 0.04	2.95 ± 0.12	2.99 ± 0.05
	15	$\searrow$	3.07 ± 0.06	3.07 ± 0.05	3.08 ± 0.05
	16	$\searrow$	3.08 ± 0.06	3.00 ± 0.05	3.01 ± 0.05
6	17	$\cap$	5.15 ± 0.24	3.02 ± 0.08	2.96 ± 0.10
	18	$\nearrow$	3.40 ± 0.08	2.99 ± 0.12	2.97 ± 0.14
	19	$\searrow$	2.92 ± 0.08	2.95 ± 0.05	2.94 ± 0.05
average			3.48	3.05	3.04
standard deviation			1.09	0.14	0.13

the thermal properties of the bearing layer: R_3 and b_3. Indeed, the inverse problem is too ill-posed if all the parameters are estimated at once. A two step procedure is therefore proposed: R_3 and b_3 are first estimated using model D. The later is fed with measurements of φ_{se} and T_{se} recorded during one oscillation period of the external air temperature. The estimated values are $R_3 = 0.28$ m^2.K.W^{-1} and $b_3 = 703$ J.K^{-1}.m^{-2}.s$^{-1/2}$. These values are then used in model C to estimate the thermal properties of the insulation layer. The results, shown in Tab 7, are as good as with model B: the thermal resistance may be estimated regardless of the evolution of $T_{\text{air,e}}$. The estimated uncertainties are of the same magnitude as the spread between experiments. Finally, it may be noted that model C supposes R_3 and b_3 perfectly known, which means that their uncertainty do not contribute to the uncertainty of $\widehat{R_1} + \widehat{R_2}$.

6 Conclusion

This paper proposes a rapid active method for the measurement of the thermal resistance of a building wall. It consists in heating the indoor air for a few hours and to apply inverse methods to measured surface heat flux and temperature. Two different types of models were implemented and compared: "white-box" models and ARX "black-box" models. The methodologies were tested on a full-scale load-bearing wall on which a conventional internal insulation system was fixed. This type of wall is representative of about three quarters of french buildings. The wall was built inside a climate chamber so that the environment could be controlled on both side. The active tests typically lasted 8 hours during which the indoor air temperature rose by about 15 K.

When the external temperature was constant, both approaches were able to estimate the thermal resistance of the insulation system (90% of the overall thermal resistance). They are based on "simple" models (models A and A') that only need measurements of the internal surface heat flux and temperature within about 6 h. The methods showed a good repeatability (5%) and the relative difference to the reference value, obtained from ISO 9869-1 [9], was below 5%. These models could not estimate the overall thermal resistance of the wall. However, this limitation is not deemed major because the insulation system represents most of the overall thermal resistance (90% here). In addition, in the case of a building retrofit, the application of the method before and after refurbishment could quantify the increase in thermal resistance because the heavy layer is unchanged.

The robustness of the method on this type of wall was assessed by undertaking experiment with unsteady external temperature. Estimations with simple models A and A' were still rather accurate if the amplitude of the external temperature variations was smaller than 5 K. Above this limit, the simple models (both "white" and "black" box) only delivered

good results if the active test was performed at moments of the day when the temperature inside the wall was rather constant. Because of material thermal inertia, this corresponds to moment when the variation of the external temperature is maximum.

More complex “white-box” models (B and C) were developed to overcome the limitations due to a varying external temperature. They lead to accurate estimations of the wall thermal resistance (below 10% difference to the reference value) in every configuration tested. However, model B requires the measurement of the temperature inside the wall, which is hardly applicable *in situ*. It was presented here for a better understanding of the problem. Model C only relies on surface measurements but requires some a priori knowledge about the bearing layer thermal properties. Though, the later may be derived from external surface measurements with a distinct model (model D). It may be noted that for lightweight walls (low thermal inertia), this two step procedure might not be required. Similarly, more complex ARX models were also tested (several inputs). They were not able to correctly estimate the thermal resistance with the proposed active procedure when the external temperature was not constant. This is due to the short measurement duration: the previous studies which successfully used similar MISO ARX models are all based on much longer datasets (from 6 to 35 consecutive days of measurement).

As a conclusion, for the studied wall, "white-box" models delivered more accurate and robust estimates than the "black-box" (ARX) models tested, except for very short measurements (around 2 h) for which the ARX approach were more stable. The models implemented and their applicability are summarized in Tab 8. The complete methodology to estimate the wall thermal resistance with an inverse method using a “white-box” model is summarized in Fig 13.

Future work will consist in validating the methods on other types of walls and other types of insulation systems (e.g. external insulation). The conclusions drawn in this study are valid for a massive wall with an internal insulation. The authors do not anticipate any difficulty to apply the same methods to lightweight walls. The best “white-box” model to choose will depend on the wall considered and the weather conditions. In addition, Bayesian inference could be used to better quantify the uncertainty over the estimation of the thermal resistance, especially for models in which some parameters are supposed perfectly known. Finally, the authors are currently working on an extension of these methods to non-homogeneous walls using infrared thermography. Indeed, the current approach is a local estimate whereas future work could extend it to distribution of thermal resistance or thermal transmittance over a wall and to thermal bridges characterization.

Acknowledgments

The authors would like to thank Etienne Hombourger, Heidi Kauffmann, Arnaud Escal and Laurent Peiffer at CEREMA-DterEst of Nancy for making available their climate chamber for our experimental campaign. They also would like to thank ANRT (Association Nationale de la Recherche et de la Technologie) for its financial support (CIFRE grant number 2017/1263).

Table 8: Summary of models (✓= yes, x = no, x✓= not true in all configurations, NA = Not Applicable).

Model	A	B	C+D	A'	B'	C'
White-box (W) or Black-box (B)	W	W	W	B	B	B
only surface measurements	✓	x	✓	✓	x	✓
only indoor measurements	✓	x	x	✓	x	x
robust to T_e variations in [0, 5] K	✓	✓	✓	✓	NA	NA
robust to T_e variations in [5, 15] K	x✓	✓	✓	x✓	NA	NA
minimum experiment duration (h)	≈ 6	≈ 6	≈ 6	≈ 2	NA	NA

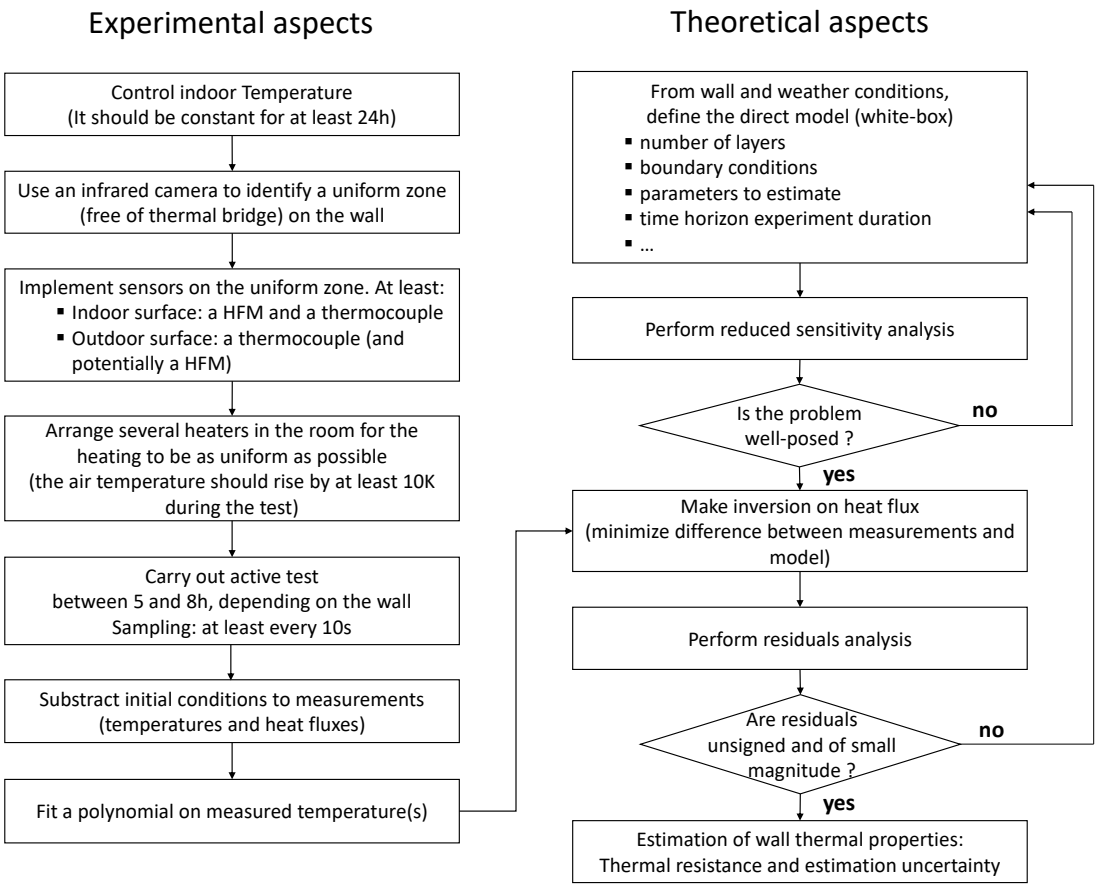

Figure 13: Summary of thermal resistance estimation methodology with the "white-box" approach.

References

[1] L. Gynther, B. Lappillone, and K. Pollier. Energy efficiency trends and policies in the household and tertiary sectors. *An analysis based on the ODYSSEE and MURE databases*, 2015.

[2] A. Stafford, M. Bell, and C. Gorse. Building Confidence – A working paper. Report 008, The Centre for Low Carbon Futures, March 2012.

[3] D. Johnston, D. Miles-Shenton, and D. Farmer. Quantifying the domestic building fabric 'performance gap'. *Building Services Engineering Research and Technology*, 36(5):614–27, 2015.

[4] M.H.A. Larbi Youcef, V. Feuillet, L. Ibos, Y. Candau, P. Balcon, and A. Filloux. Quantitative diagnosis of insulated building walls of restored old constructions using active infrared thermography. *Quantitative InfraRed Thermography Journal*, 8(1):65–87, 2011.

[5] D. Bienvenido-Huertas, J. Moyano, D. Marín, and R. Fresco-Contreras. Review of in situ methods for assessing the thermal transmittance of walls. *Renewable and Sustainable Energy Reviews*, 102:356–371, 2019.

[6] N. Soares, C. Martins, M. Gonçalves, P. Santos, L.S. da Silva, and J.J. Costa. Laboratory and in-situ non-destructive methods to evaluate the thermal transmittance and behavior of walls, windows, and construction elements with innovative materials: A review. *Energy and Buildings*, 182:88–110, 2019.

[7] M. Teni, H. Krstić, and P. Kosiński. Review and comparison of current experimental approaches for in-situ measurements of building walls thermal transmittance. *Energy and Buildings*, page 109417, 2019.

[8] ISO 8990:1996. Thermal insulation – Determination of steady-state thermal transmission properties – Calibrated and guarded hot box. *International Standards Organisation*, 1996.

[9] ISO 9869-1:2014. Thermal insulation – Building elements – In-situ measurement of thermal resistance and thermal transmittance – Part 1: Heat flow meter method. *International Standards Organisation*, 2014.

[10] G. Ficco, F. Iannetta, E. Ianniello, F.R. Alfano, and M. Dell'Isola. U-value in situ measurement for energy diagnosis of existing buildings. *Energy and Buildings*, 104:108–121, 2015.

[11] A. Rasooli, L. Itard, and C.I. Ferreira. A response factor-based method for the rapid in-situ determination of walls thermal resistance in existing buildings. *Energy and Buildings*, 119:51–61, 2016.

[12] L. Evangelisti, C. Guattari, and F. Asdrubali. Influence of heating systems on thermal transmittance evaluations: Simulations, experimental measurements and data post-processing. *Energy and Buildings*, 168:180–190, 2018.

[13] K. Gaspar, M. Casals, and M. Gangolells. A comparison of standardized calculation methods for in situ measurements of façades U-value. *Energy and Buildings*, 130:592–599, 2016.

[14] K. Gaspar, M. Casals, and M. Gangolells. Review of criteria for determining HFM minimum test duration. *Energy and Buildings*, 176:360–370, 2018.

[15] C.A. Balaras and A.A. Argiriou. Infrared thermography for building diagnostics. *Energy and Buildings*, 34(2):171–83, 2002.

[16] A. Kylili, P.A. Fokaides, P. Christou, and S.A. Kalogirou. Infrared thermography (IRT) applications for building diagnostics: A review . *Applied Energy*, 134(0):531–49, 2014.

[17] E. Barreira and V.P. de Freitas. Evaluation of building materials using infrared thermography. *Construction and building materials*, 21(1):218–224, 2007.

[18] B. Lehmann, K.G. Wakili, Th. Frank, B.V. Collado, and Ch Tanner. Effects of individual climatic parameters on the infrared thermography of buildings. *Applied Energy*, 110:29–43, 2013.

[19] ISO 13187:1999. Thermal Performance of Buildings - Qualitative Detection of Thermal Irregularities in Building Envelopes - Infrared method (ISO 6781:1983 Modified). *International Standards Organisation*, 1999.

[20] S.M. Ocaña, I.C. Guerrero, and I.G. Requena. Thermographic survey of two rural buildings in Spain. *Energy and Buildings*, 36(6):515–523, 2004.

[21] N. Garcez, N. Lopes, J. de Brito, and J. Silvestre. System of inspection, diagnosis and repair of external claddings of pitched roofs. *Construction and Building Materials*, 35:1034–1044, 2012.

[22] A. Menezes, M.G. Gomes, and I. Flores-Colen. In-situ assessment of physical performance and degradation analysis of rendering walls. *Construction and Building Materials*, 75:283–292, 2015.

[23] T. Taylor, J. Counsell, and S. Gill. Combining thermography and computer simulation to identify and assess insulation defects in the construction of building façades. *Energy and Buildings*, 76:130–142, 2014.

[24] ISO 9869-2:2018. Thermal insulation – Building elements – In-situ measurement of thermal resistance and thermal transmittance – Part 2: Infrared method for frame structure dwelling. *International Standards Organisation*, 2018.

[25] S. Kato, K. Kuroki, and S. Hagihara. Method of in-situ measurement of thermal insulation performance of building elements using infrared camera. In *6th International Conference on Indoor Air Quality, Ventilation & Energy Conservation in Buildings-IAQVEC*, volume 2007. Citeseer, 2007.

[26] R. Madding. Finding R-values of stud frame constructed houses with IR thermography. *Proc., InfraMation 2008*, pages 261–277, 2008.

[27] B. Tejedor, M. Casals, M. Gangolells, and X. Roca. Quantitative internal infrared thermography for determining in-situ thermal behaviour of façades. *Energy and Buildings*, 151:187–197, 2017.

[28] B. Tejedor, M. Casals, M. Macarulla, and A. Giretti. U-value time series analyses: Evaluating the feasibility of in-situ short-lasting IRT tests for heavy multi-leaf walls. *Building and Environment*, 159:106123, 2019.

[29] P. A Fokaides and S.A Kalogirou. Application of infrared thermography for the determination of the overall heat transfer coefficient (U-Value) in building envelopes. *Applied Energy*, 88(12):4358–4365, 2011.

[30] ISO 6946:2017. Building components and building elements - Thermal resistance and thermal transmittance - Calculation methods. *International Standards Organisation*, 2017.

[31] I. Danielski and M. Fröling. Diagnosis of buildings thermal performance-a quantitative method using thermography under non-steady state heat flow. *Energy Procedia*, 83:320–329, 2015.

[32] R. Albatici and A.M Tonelli. Infrared thermovision technique for the assessment of thermal transmittance value of opaque building elements on site. *Energy and Buildings*, 42(11):2177–2183, 2010.

[33] R. Albatici, A.M Tonelli, and M. Chiogna. A comprehensive experimental approach for the validation of quantitative infrared thermography in the evaluation of building thermal transmittance. *Applied energy*, 141:218–228, 2015.

[34] I. Nardi, S. Sfarra, and D. Ambrosini. Quantitative thermography for the estimation of the U-value: state of the art and a case study. In *Journal of Physics: Conference Series*, volume 547, page 012016. IOP Publishing, 2014.

[35] G. Dall'O, L. Sarto, and A. Panza. Infrared screening of residential buildings for energy audit purposes: results of a field test. *Energies*, 6(8):3859–3878, 2013.

[36] D. Bienvenido-Huertas, J. Bermúdez, J.J. Moyano, and D. Marín. Influence of ICHTC correlations on the thermal characterization of façades using the quantitative internal infrared thermography method. *Building and Environment*, 149:512–525, 2019.

[37] D. Bienvenido-Huertas, J. Bermúdez, J. Moyano, and D. Marín. Comparison of quantitative IRT to estimate U-value using different approximations of ECHTC in multi-leaf walls. *Energy and Buildings*, 184:99–113, 2019.

[38] L. Ibos, J.P. Monchau, V. Feuillet, and Y. Candau. A comparative study of in-situ measurement methods of a building wall thermal resistance using infrared thermography. In *Twelfth International Conference on Quality Control by Artificial Vision 2015*, volume 9534, page 95341I. International Society for Optics and Photonics, 2015.

[39] C. Roulet, J. Gass, and I. Marcus. In situ U-value measurement: reliable results in shorter time by dynamic interpretation of the measured data. *Thermal Performance of the Exterior Envelopes of Buildings III; ASHRAE Transactions: Atlanta, GA, USA*, pages 777–784, 1987.

[40] G. Anderlind. Multiple regression analysis of in situ thermal measurements, Study of an attic insulated with 800 mm loose fill insulation. *Journal of Thermal Insulation and Building Envelopes*, 16(1):81–104, 1992.

[41] G. Anderlind. *Dynamic Thermal Models: Two Dynamic Models for Estimating Thermal Resistance and Heat Capacity from in Situ Measurements*. Byggforskningsrådet, 1996.

[42] O. Gutschker. Parameter identification with the software package LORD. *Building and Environment*, 43(2):163–169, 2008.

[43] P.H Baker and H. Van Dijk. PASLINK and dynamic outdoor testing of building components. *Building and Environment*, 43(2):143–151, 2008.

[44] M.J. Jiménez, B. Porcar, and M.R. Heras. Application of different dynamic analysis approaches to the estimation of the building component U value. *Building and Environment*, 44(2):361–367, 2009.

[45] A.H. Deconinck and S. Roels. Comparison of characterisation methods determining the thermal resistance of building components from onsite measurements. *Energy and Buildings*, 130:309–320, 2016.

[46] A.H. Deconinck and S. Roels. A maximum likelihood estimation of the thermal resistance of a cavity wall from on-site measurements. *Energy Procedia*, 78:3276–3281, 2015.

[47] I. Naveros, P. Bacher, D.P. Ruiz, M.J. Jiménez, and H. Madsen. Setting up and validating a complex model for a simple homogeneous wall. *Energy and Buildings*, 70:303–317, 2014.

[48] P. Bacher and H. Madsen. Identifying suitable models for the heat dynamics of buildings. *Energy and Buildings*, 43(7):1511–1522, 2011.

[49] P. Biddulph, V. Gori, C. A Elwell, C. Scott, C. Rye, R. Lowe, and T. Oreszczyn. Inferring the thermal resistance and effective thermal mass of a wall using frequent temperature and heat flux measurements. *Energy and Buildings*, 78:10–16, 2014.

[50] V. Gori, V. Marincioni, P. Biddulph, and C.A Elwell. Inferring the thermal resistance and effective thermal mass distribution of a wall from in situ measurements to characterise heat transfer at both the interior and exterior surfaces. *Energy and Buildings*, 135:398–409, 2017.

[51] V. Gori and C.A. Elwell. Estimation of thermophysical properties from in-situ measurements in all seasons: Quantifying and reducing errors using dynamic grey-box methods. *Energy and Buildings*, 167:290–300, 2018.

[52] L. De Simon, M. Iglesias, B. Jones, and C. Wood. Quantifying uncertainty in thermophysical properties of walls by means of Bayesian inversion. *Energy and Buildings*, 177:220–245, 2018.

[53] D. Bienvenido-Huertas, J. Moyano, C.E. Rodríguez-Jiménez, and D. Marín. Applying an artificial neural network to assess thermal transmittance in walls by means of the thermometric method. *Applied energy*, 233:1–14, 2019.

[54] D. Bienvenido-Huertas, C. Rubio-Bellido, J.L. Pérez-Ordóñez, and J. Moyano. Optimizing the evaluation of thermal transmittance with the thermometric method using multilayer perceptrons. *Energy and Buildings*, 198:395–411, 2019.

[55] D. Bienvenido-Huertas, J.L. Pérez-Ordóñez, J. Moyano, and S. Seara-Paz. Towards an in-situ evaluation methodology of thermal resistance of basement walls in buildings. *Energy and Buildings*, 208:109643, 2020.

[56] L. Ljung. *System identification: theory for the user*. 1999.

[57] M.J. Jiménez, H. Madsen, and K.K. Andersen. Identification of the main thermal characteristics of building components using MATLAB. *Building and Environment*, 43(2):170–180, 2008.

[58] I. Naveros, C. Ghiaus, D.P. Ruiz, and S. Castano. Physical parameters identification of walls using ARX models obtained by deduction. *Energy and Buildings*, 108:317–329, 2015.

[59] E. Lambie and D. Saelens. The thermal resistance of retrofitted building components based on in-situ measurements. 2018.

[60] M.J. Jimenez and H. Madsen. Models for describing the thermal characteristics of building components. *Building and Environment*, 43(2):152–162, 2008.

[61] H. Madsen, P. Bacher, G. Bauwens, A.H. Deconinck, G. Reynders, S. Roels, E. Himpe, and G. Lethé. Thermal performance characterization using time series data-IEA EBC Annex 58 Guidelines. 2015.

[62] M. Senave, G. Reynders, P. Bacher, S. Roels, S. Verbeke, and D. Saelens. Towards the characterization of the heat loss coefficient via on-board monitoring: Physical interpretation of ARX model coefficients. *Energy and Buildings*, 195:180–194, 2019.

[63] M. Senave, G. Reynders, B. Sodagar, S. Verbeke, and D. Saelens. Mapping the pitfalls in the characterisation of the heat loss coefficient from on-board monitoring data using ARX models. *Energy and Buildings*, 197:214–228, 2019.

[64] E. Lambie, M. Senave, and D. Saelens. The co-heating test as a means to evaluate the efficiency of thermal retrofit measures applied on residential buildings. *http://ibpc2018. org/proceedings/*, pages 953–958, 2018.

[65] A. Gagliano, F. Patania, F. Nocera, and C. Signorello. Assessment of the dynamic thermal performance of massive buildings. *Energy and Buildings*, 72:361–370, 2014.

[66] R. Ricciu, F. Ragnedda, A. Galatioto, S. Gana, L.A. Besalduch, and A. Frattolillo. Thermal properties of building walls: Indirect estimation using the inverse method with a harmonic approach. *Energy and Buildings*, 187:257–268, 2019.

[67] ISO 13786:2007. Thermal performance of building components–Dynamic thermal characteristics–Calculation methods. *International Organization for Standardization*, 2007.

[68] Á. Lakatos. Comprehensive thermal transmittance investigations carried out on opaque aerogel insulation blanket. *Materials and Structures*, 50(1):2, 2017.

[69] J. Meulemans, F. Alzetto, D. Farmer, and C. Gorse. QUB/e: A Novel Transient Experimental Method for in situ Measurements of the Thermal Performance of Building Fabrics. In *Building Information Modelling, Building Performance, Design and Smart Construction*, pages 115–127. Springer, 2017.

[70] J. Meulemans. An assessment of the QUB/e method for fast in situ measurements of the thermal performance of building fabrics in cold climates. In *Cold Climate HVAC Conference*, pages 317–326. Springer, 2019.

[71] Vasileos Sougkakis, Johann Meulemans, Florent Alzetto, Christopher Wood, Mark Gillott, and Thomas Cox. An assessment of the qub method for predicting the whole building thermal performance under actual operating conditions. 2017.

[72] A. Rasooli and L. Itard. In-situ rapid determination of walls' thermal conductivity, volumetric heat capacity, and thermal resistance, using response factors. *Applied energy*, 253:113539, 2019.

[73] S. Rouchier. Solving inverse problems in building physics: An overview of guidelines for a careful and optimal use of data. *Energy and Buildings*, 166:178–195, 2018.

[74] Y. Yang, T.V. Wu, A. Sempey, J. Dumoulin, and J.C. Batsale. Short time non-destructive evaluation of thermal performances of building walls by studying transient heat transfer. *Energy and Buildings*, 184:141–151, 2019.

[75] X. Maldague. Theory and practice of infrared technology for nondestructive testing. *Ed. Wiley-Intersciences*, New York, 2001.

[76] K. Chaffar, A. Chauchois, D. Defer, and L. Zalewski. Thermal characterization of homogeneous walls using inverse method. *Energy and Buildings*, 78:248–255, 2014.

[77] H. Preston-Thomas. The international temperature scale of 1990 (ITS-90). *metrologia*, 27(1):3, 1990.

[78] IEC ISO and BIPM OIML. Guide to the Expression of Uncertainty in Measurement. *Geneva, Switzerland*, 122, 1995.

[79] J.V. Beck, B. Blackwell, and C. R St Clair Jr. *Inverse heat conduction: Ill-posed problems*. James Beck, 1985.

[80] H.R.B. Orlande, O. Fudym, D. Maillet, and R.M. Cotta. *Thermal measurements and inverse techniques*. CRC Press, 2011.

[81] J. Hadamard. Lectures on Cauchy's Problem in Linear Partial Differential Equations, Yale Univ. *Press. New Haven*, 1923.

[82] D. Maillet, S. André, J.C. Batsale, A. Degiovanni, and C. Moyne. *Thermal quadrupoles: solving the heat equation through integral transforms*. John Wiley & Sons Inc, 2000.

[83] F.R. De Hoog, J.H. Knight, and A.N. Stokes. An improved method for numerical inversion of Laplace transforms. *SIAM Journal on Scientific and Statistical Computing*, 3(3):357–366, 1982.

[84] K. Levenberg. A method for the solution of certain nonlinear problems in least squares. *Quarterly of applied mathematics*, 2(2):164–168, 1944.

[85] D.W. Marquardt. An algorithm for least-squares estimation of nonlinear parameters. *Journal of the society for Industrial and Applied Mathematics*, 11(2):431–441, 1963.

[86] J.J. Moré. The Levenberg-Marquardt algorithm: implementation and theory. In *Numerical analysis*, pages 105–116. Springer, 1978.

[87] S.E. Gustafsson. Transient plane source techniques for thermal conductivity and thermal diffusivity measurements of solid materials. *Review of scientific instruments*, 62(3):797–804, 1991.

[88] JC Jones and M Wade. On the thermal diffusivity of insulating glass wool. *Journal of fire sciences*, 18(1):74–77, 2000.